Journal of the Microelectronics & Packaging Society
Vol. 9, No. 4, p. 35-45. 2002

언더필/칩 계면의 응력 해석

박지은 · Iwona Jasiuk · 이호영*

조지아공대 기계공학부
*서울대학교 기계항공공학부

Analysis of Stresses Along the Underfill/Chip Interface

Ji Eun Park, Iwona Jasiuk and Ho-Young Lee*

School of Mechanical Engineering, Georgia Institute of Technology
*School of Mechanical and Aerospace Engineering, Seoul National University

초 록: 열하중에 의한 언더필/칩 계면의 응력을 유한요소법을 이용하여 구하였다. 먼저 실리카 입자의 부피 분율이 언더필 재료의 물성에 미치는 영향을 알아보기 위하여 세 가지 재료 세트에 대하여 실리카 입자의 부피 분율에 따른 영계수, 포아슨비, 영팽창 계수를 Mori-Tanaka 방법을 이용하여 계산하였고, 언더필과 칩이 형성하는 edge 및 wedge에 대한 singularity를 계산하였다. 그 다음에는 앞에서 계산한 재료물성치를 가지고 실리카 입자의 부피 분율에 따른 언더필/칩 계면의 응력을 몇 가지 플립칩 형상에 대하여 살펴보았다. 언더필이 균일한 재료라는 가정과 플립칩 어셈블리를 구성하고 있는 재료들이 선형탄성적거동을 하고 등방성을 보이며 그들의 성질이 온도에 무관하다는 가정 하에 다섯 가지의 플립칩 어셈블리 모델이 고려되었다.

Abstract: The stresses of the underfill/chip interface due to thermal loading was studied using the finite element method. At first, the effective properties of underfill for several volume fractions of silica particles were calculated by Mori-Tanaka method for three different material sets, and the parameters of singularity for the bimaterial edge and the bimaterial wedge were calculated. Consequently, the stresses at the underfill/chip interface with volume fraction of silica particles were investigated. Five different geometric models of flip-chip assembly involving two kinds of bimaterial strips and three kinds of three-layer models were considered under the assumption that the underfill is homogeneous. It was assumed that all components of the flip-chip assembly were linear elastic and isotropic, and their properties were temperature independent. The analysis was conducted in the context of the uncoupled plane thermo-elasticity under a plane strain assumption.

Keywords: stress, underfill, chip, interface, thermal loading, singularity, bimaterial, finite element method

1. Introduction

There are three basic types of connections between integrated circuits (ICs) and packages or modules: wire bond, Tape Automated Bonding (TAB) and flip-chip bonding. Among them, the flip-chip bonding becomes the most promising method because of the minimized interconnect distance and very high chip density. However, this method has some problems. One of the biggest challenges in the flip-chip bonding is to develop a thermally compatible encapsulant to reduce the deformation at the interfaces of underfill/chip and solder bumps/chip due to a large mismatch in coefficient of thermal expansion (CTE) between those materials.

A chip is attached to a substrate by solder joints

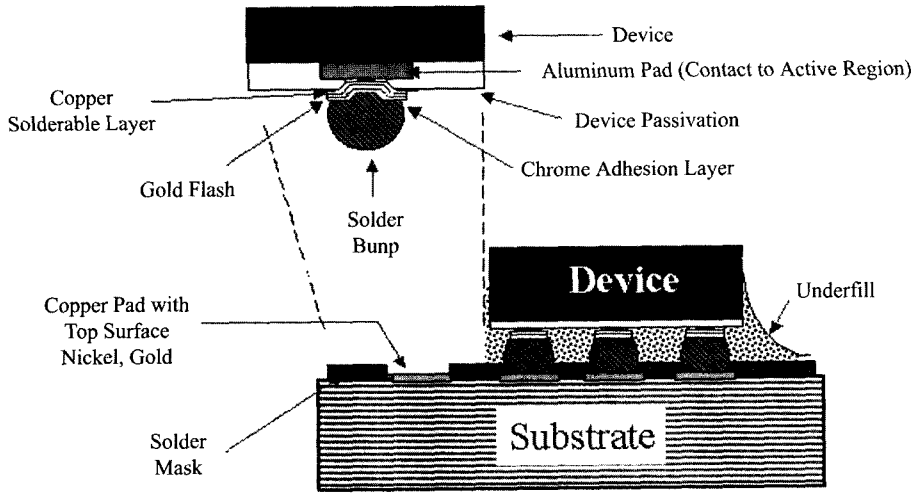

Fig. 1. The flip-chip assembly.

that in turn are surrounded by an underfill material (encapsulant) using Controlled Collapse Chip Connection (C4) process developed by IBM. The underfill protects the solder bumps from the environment by reducing deformation in solder joints when the device is subjected to temperature changes. A schematic drawing of the flip-chip assembly is shown in Fig. 1. The flip-chip assembly undergoes thermal loads during post-curing and its operational life. Since the components of the flip-chip device have different coefficients of thermal expansion (CTE), several failures may occur with different modes. They include cracking on the top of the chip due to the chip bending, microcracking in the underfill, and delamination at the underfill/chip, the underfill/substrate, or the chip/solder bumps interfaces. Delamination at the chip/solder bumps interfaces is commonly observed. The propagation of crack caused by a prior delamination at the underfill/chip interface exposes solder joints and causes premature device failures.

In the present work, the attention is concentrated on the underfill/chip interface. At first, the effective properties of underfill and the parameters of singularity for the bimaterial edge and the bimaterial wedge were calculated. And next, the stresses of the underfill/chip interface were predicted using finite element method. For simplicity, solder bumps are excluded in the analysis. This is justified because the underfill/chip interface is away from solder bumps.

2. Theoretical Background

2.1 Effective Properties

Several approaches are available to predict effective elastic moduli of composite materials. They include variational approaches leading to bounds[1], effective medium theories (e.g., self-consistent method by Budiansky[2] and Hill[3]; Mori-Tanaka method by Mori and Tanaka[4] and Benveniste[5]), analytical solutions for idealized geometric models, and numerical approaches. These methods are summarized in Christensen[6], Mura[7], Hashin[8], and other references.

In the present work, the effective properties of underfill were evaluated by utilizing the Mori-Tanaka method. By this method, the effective bulk modulus (K^*) of a matrix-inclusion composite with spherical particles is given by

$$K^* = K_1 + \frac{f(K_2 - K_1)K_1}{(1-f)(K_2 - K_1)\gamma_1 + K_1} \tag{1}$$

where $\gamma_1 = 3K_1/(3K_1 + 4\mu_1)$, f, is the volume fraction of particles, $K_i (i = 1, 2)$ are bulk moduli, $\mu_i (i = 1, 2)$ are shear moduli, and subscripts 1 and 2 stand for matrix and particles, respectively. The effective shear modulus (μ^*) is given by

$$\mu^* = \mu_1 + \frac{f(\mu_2 - \mu_1)\mu_1}{(1-f)(\mu_2 - \mu_1)\beta_1 + \mu_1} \tag{2}$$

where $\beta_1 = 6(K_1 + 2\mu_1)/[5(3K_1 + 4\mu_1)]$.

The effective coefficient of thermal expansion (CTE), α^*, is expressed as

$$\alpha^* = \alpha_1 + (\alpha_2 - \alpha_1)\frac{(1/K^* - 1/K_1)}{(1/K_2 - 1/K_1)} \quad (3)$$

where $\alpha_1 (i = 1, 2)$ are individual thermal expansion coefficients. Qu and Wong[9] also used this method to estimate the effective elastic modulus of underfill with particles and measured these values experimentally. They observed excellent agreement between theoretically predicted data and their experimental data.

2.2 Stress Singularity

2.2.1 Edge of a bimaterial Strip

The stresses along an interface of dissimilar materials become singular at a traction-free edge. There have been numerous works on stress singularity calculations for a bimaterial strip for linear elastic materials. Williams[10] found the modulus of the singularity behavior of the stress remains proportional to the inverse square root of the distance from the point of the crack. Bogy[11], and Bogy and Sternberg[12] solved the plane problem of two dissimilar orthogonal elastic wedges, bonded together and subjected to surface traction on the boundary and, found the asymptotic behavior of the elastic solution at the edge. He used the Mellin transform with the Airy stress function. Bogy[13] expressed the stress field in bonded quarter planes of different elastic materials due to mechanical loading in terms of Dundurs constants, α and β, defined by Dundurs[14] such as

$$\alpha = \frac{\Gamma(\chi_1 + 1) - (\chi_2 + 1)}{\Gamma(\chi_1 + 1) + (\chi_2 + 1)} = \frac{C_1 - C_2}{C_1 + C_2} \quad (4)$$

$$\beta = \frac{\Gamma(\chi_1 - 1) - (\chi_2 - 1)}{\Gamma(\chi_1 + 1) + (\chi_2 + 1)} = \frac{A_1 - A_2}{4(C_1 + C_2)} \quad (5)$$

where $\Gamma = \mu_1/\mu_2$, and Kolosov constant χ is given as

$$\chi = 3 - 4\nu \text{ for plane strain} \quad (6)$$

$$\chi = \frac{3 - 4\nu}{1 + \nu} \text{ for plane stress} \quad (7)$$

where μ and ν denote shear modulus and Poisson's ratio, respectively. The bulk compliance A and uniaxial compliance C are defined as

$$A = \frac{(\chi - 1)}{2G} \quad (8)$$

$$C = \frac{(\chi + 1)}{8G} \quad (9)$$

He reported that the stress field is of order $r^{-\lambda}$, $\log r$, and 1 where r is the distance from the edge depending on the values of α and β where λ depends on the elastic constants.

$$r^{-\lambda} \quad \text{when } \alpha(\alpha - 2\beta) > 0 \quad (10)$$

$$\log r \quad \text{when } \alpha(\alpha - 2\beta) = 0 \quad (11)$$

$$1 \quad \text{when } \alpha(\alpha - 2\beta) < 0 \quad (12)$$

The material sets in our research satisfy the condition in Eq. (10). Thus, stress field at a bimaterial interface at the edge can be expressed in the form

$$\sigma_{ij} = C_{ij} r^{-\lambda} \quad (13)$$

where C_{ij} depends on geometry, material mismatch and loading and is obtained by solving a boundary value problem, while the parameter λ depends only on the elastic constants of two materials and the geometry at the edge. When $\lambda > 0$, then the stress field is singular. Chung and Eischen[15] calculated the degree of the stress singularity that occurs at the termination of an interface between materials exhibiting bilinear stress-strain response under plane strain conditions and Lee and Jasiuk[16] studied an asymptotic behavior of stresses in semi-infinite bimaterial strips.

2.2.2 Wedge of a Bimaterial Strip

Theocaris[17] solved the plane problem of a composite body consisting of many dissimilar isotropic, homogeneous and elastic wedges with a number of corners. Dempsey and Sinclair[18] studied the singular behavior at the vertex of a bimaterial wedge. Groth[19] found that the singular stresses at interface corners in bonded lab joints assuming linear elasticity. Gu and Belytschko[20] presented a numerical procedure to determine the stress singularity at the vertex of a two

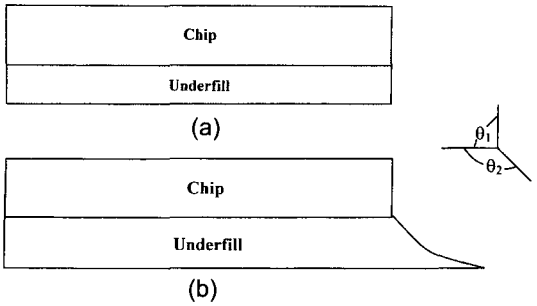

Fig. 2. Sketches of bimaterial strips with (a) a straight edge and (b) a wedge.

material wedge using an eigenfunction expansion technique. Pageau *et al.*[21] developed a finite element formulation for determining the order of the singularity and the angular variation of the inplane displacement and stress fields around a singular point in anisotropic materials. Vroonhoven[22] and Fan *et al.*[23] analyzed the nature of stress singularity in bimaterial wedges. The general characteristic equation for determining the order of the singularity is given as

$$D(\theta_1, \theta_2, \alpha, \beta, \lambda) = 0 \tag{14}$$

where θ_1 and θ_2 are defined in Fig. 2, α and β are the Dundurs constants and λ is the parameter of stress singularity. The general characteristic equation for angular corner of bimaterial wedge is following[22]:

$$\begin{aligned}&16[\sin^2(\theta_1 p)-p^2\sin^2(\theta_1)][\sin^2(\theta_2 p)-p^2\sin^2(\theta_2)]\beta^2\\&+16p^2\{\sin^2(\theta_1)[\sin^2(\theta_2 p)-p^2\sin^2(\theta_2)]+\sin^2(\theta_1)\\&[\sin^2(\theta_1 p)-p^2\sin^2(\theta_1)]\}\alpha\beta+\{16p^2(p^2-1)\sin^2(\theta_1)\\&\sin^2(\theta_2)-4[p^2\sin^2(\theta_2+\theta_1)-\sin^2 p(\theta_2+\theta_1)]\}\alpha^2\\&+16p^2[\sin^2(\theta_1)\sin^2(\theta_2 p)-\sin^2(\theta_2)\sin^2(\theta_1 p)]\beta\\&+8\{-2p^2[\sin^2(\theta_1)\sin^2(\theta_2 p)-\sin^2(\theta_2)\sin^2(\theta_1 p)]\\&+[\sin^2(\theta_2 p)-p^2\sin^2(\theta_2)]-[\sin^2(\theta_1 p)-p^2\sin^2(\theta_1)]\}\\&\alpha-4p^2\sin^2(\theta_1-\theta_2)+4p^2\sin^2 p(\theta_1-\theta_2)=0\end{aligned} \tag{15}$$

where $p = \lambda + 1$.

3. Problem Setup

According to Wang *et al.*[24], the creep behavior of the underfill does not have a significant influence on the failure of a flip-chip package. It is true that the substrate (FR-4) is usually anisotropic, however, for simplicity, it is acceptable to assume that the substrate is isotropic because we are interested in the underfill/chip interface, which is away from the substrate. It is also assumed that material properties of underfill are independent of temperature. This assumption is valid as long as the temperature during the thermal cycle is quite below the glass transition temperature. The analysis is conducted in the context of the uncoupled plane thermo-elasticity under a plane strain assumption. Thus, the model is the cross-sectioned flip-chip device represented by a long cylinder. This two-dimensional (2D) plane strain assumption is not valid when the cross-section is close to the corner of the assembly because of the three dimensional (3D) corner effects. However, we can still obtain consistent results using the 2D plane strain model with ones from complex 3D models when we are away from corners. This observation is supported by Michaelides and Sitaraman[25], Hanna and Sitaraman[26], Yeh *et al.*[27], and others. The analysis is two-dimensional and is conducted in the context of uncoupled thermo-elasticity under plane strain. One additional assumption is that there is no initial residual stress in the model, i.e. it is assumed that our model is at a zero stress prior to applying thermal loadings. This assumption is used in most electronic packaging papers for simplicity. The idealized package structure is subjected to a temperature change equal to −100°C. This loading may represent post-curing thermal loading since the flip-chip device is cured at around 130°C and cooled to room temperature. We conducted the calculations using the finite element code ABAQUS, and adopted IDEAS to generate finite element meshes. We used the 8 node quadratic elements in the finite element analysis.

To reduce the CTE mismatch of the components (chip, underfill and substrate), particles of the similar material as the chip are put in the underfill. Thus, the underfill is a composite material with a polymer matrix and silica particles. The heterogeneity of underfill is not important in the analysis of average stresses in the system but it is crucial in the studies of failure/damage since the fracture is a local phenomenon occurring at very small scales at which the

micro-structural details strongly contribute. In order to make the underfill properties compatible with the rest of the assembly, silica particles are dispersed in the encapsulant.

It was assumed that the underfill is a homogeneous material having effective properties of a composite. In the parametric study we considered a range of volume fractions of silica particles in the underfill. The effective properties of underfill are calculated by Mori-Tanaka method. With that assumption, we investigated how the interfacial stresses at the underfill/chip interface are influenced by varying volume fraction of silica particles in underfill and by the different geometric models of flip-chip devices such as finite bimaterial strips and three-layer models with different strip lengths and curvature of the underfill.

4. Results and Discussion

4.1 Effective Properties

The effective properties for several volume fractions of silica particles in the underfill were calculated. Table 1 shows the material sets used in the calculation of effective properties and stress analyses. The material sets 1 and 2 are very similar except the material properties of underfill matrix. The material set 2 has the lower Young's modulus and Poisson's ratio. The material set 3, which was cited by Mahidhara *et al.*[28], was employed to observe the consequence of material mismatch quantities in spite of the exceedingly large material mismatches.

It was assumed that particles are spherical in shape for the analytical calculations of effective properties of underfill. The Mori-Tanaka method is used to find the effective bulk modulus (K^*), shear modulus (μ^*), and CTE (α^*). Those material properties are calculated by the Eqns. (1)-(3) and the effective Young's modulus (E^*) and the effective Poisson's ratio (ν^*) are obtained from the K^* and μ^*.

$$E^* = \frac{9K^*\mu^*}{3K^* + \mu^*} \tag{16}$$

$$\nu^* = \frac{3K^* - 2\mu^*}{6K^* + 2\mu^*} \tag{17}$$

The E^*, ν^*, and α^* are plotted as functions of silica particle volume fraction, f, in Figs. 3-5 for the material sets 1, 2 and 3. Note that the effective properties of underfill were calculated for a complete range of particle volume fractions, including $f = 1$. The maximum packing of spherical-shaped particles of the same diameter is $\pi\sqrt{2}/6$ (~0.74) for cubical packing and can reach a value close to unity when gradation in particle size is present. In a typical underfill, the f is about 0.4 and the particles do vary in diameter. The size of particles is not accounted for in the Mori-Tanaka effective medium theory.

These analytical calculations illustrate that as the f

Table 1. Material sets 1, 2 and 3 used in bimaterial strips and three-layer cases

		Substrate (FR-4)	Chip (Silicon)	Underfill (Polymer-epoxy)	Particle (Silica)
Set 1	E (GPa)	12.4	186	4.50	73.0
	ν	0.33	0.27	0.33	0.17
	α (ppm/°C)	18.0	3.00	60.0	0.50
Set 2	E (GPa)	12.4	186	2.10	73.0
	ν	0.33	0.27	0.25	0.17
	α (ppm/°C)	18.0	3.00	60.0	0.50
		Chip and Particles (Silicon)	Underfill matrix (Polymer)		Underfill (Composite)
Set 3[28]	E	186 GPa	6.89 MPa		18.5 MPa
	ν	0.27	0.49		0.484
	α (ppm/°C)	3	180		108

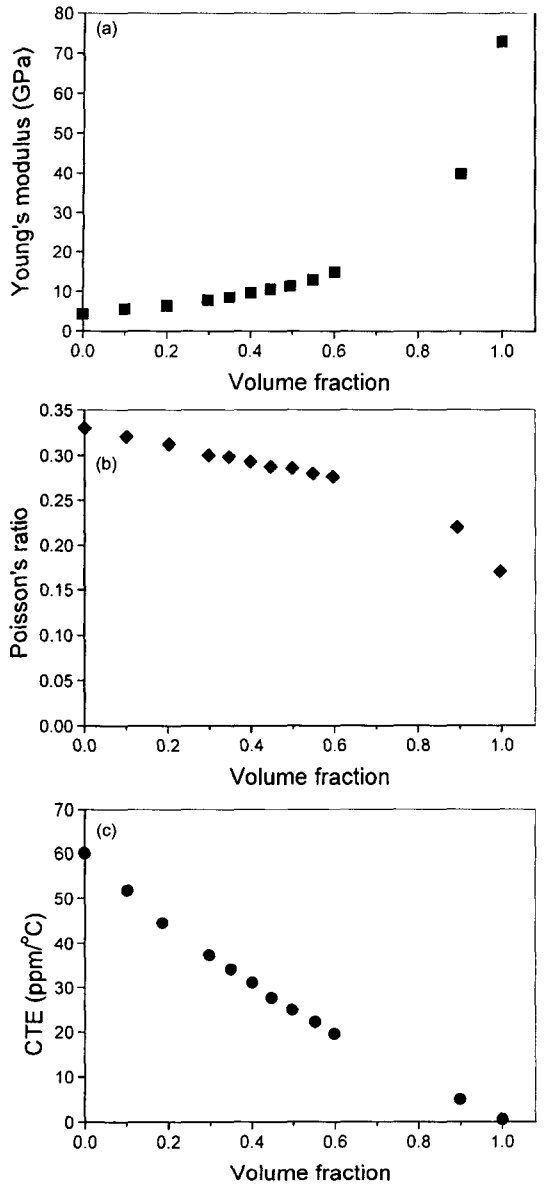

Fig. 3. Effective material properties of the material set 1: (a) effective Young's modulus, (b) effective Poisson's ratio, and (c) effective coefficient of thermal expansion (CTE).

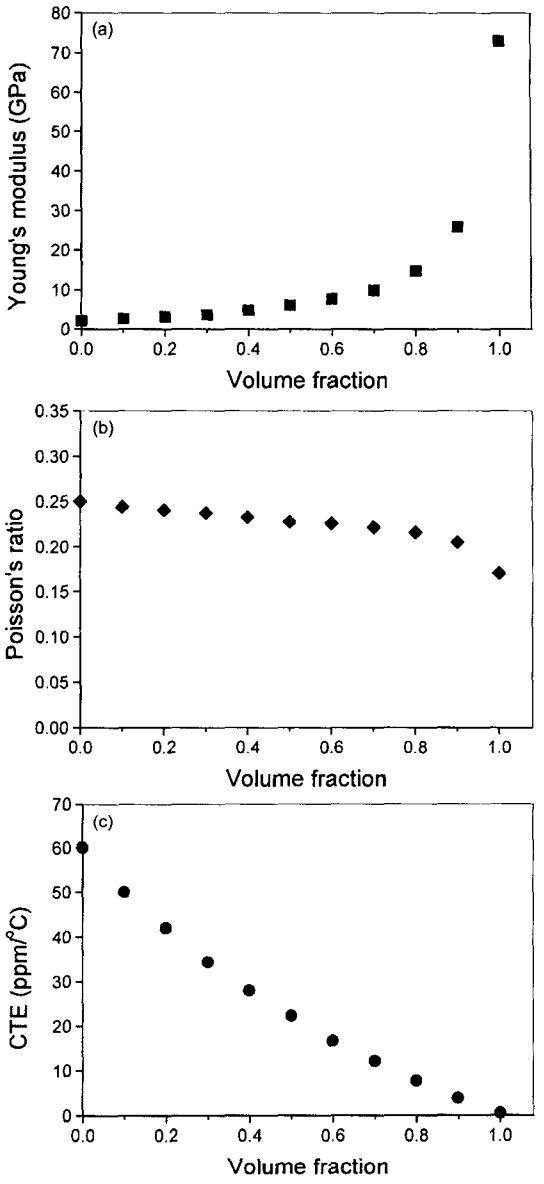

Fig. 4. Effective material properties of the material set 2: (a) effective Young's modulus, (b) effective Poisson's ratio, and (c) effective coefficient of thermal expansion (CTE).

increases, the effective Young's modulus of underfill increases, while the effective Poisson's ratio and the effective CTE decreases for all material sets. For the material set 1 and 2, all three material properties change gradually as the f increases. However, for the material set 3, the effective Young's modulus and the effective Poisson's ratio do not change much until the f reaches 0.9 and after that point, those properties alter abruptly. Since the underfill matrix of the material set 3 has unreasonably high CTE and Poisson's ratio and low Young's modulus, the material mismatches between the matrix and particles are too

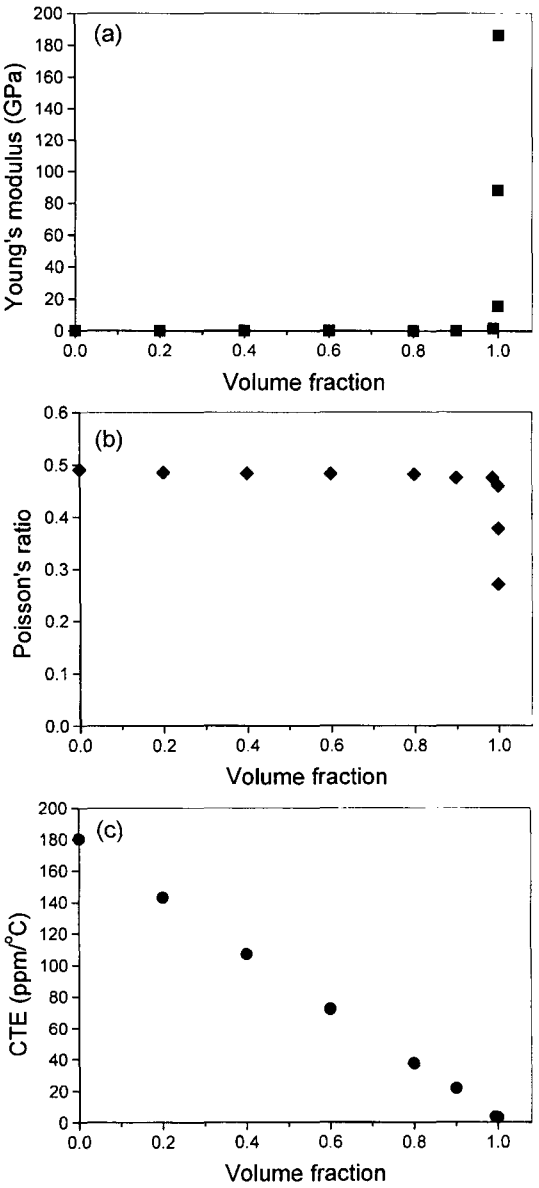

Fig. 5. Effective material properties of the material set 3: (a) effective Young's modulus, (b) effective Poisson's ratio, and (c) effective coefficient of thermal expansion (CTE).

large. That's why the effective Young's modulus and the effective Poisson's ratio show how the peculiar trends compared to the material sets 1 and 2.

4.2 Singularity of Stresses

The parameters of stress singularity λ were calculated as a function of f in underfill for two different geometries: a bimaterial with a straight edge[16,29] and a bimaterial with an angular corner[17,22,23]. The sketches of these two geometries are shown in Fig. 2.

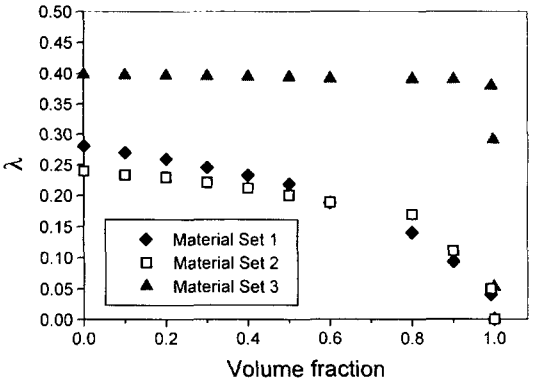

Fig. 6. Stress singularity vs. volume fraction of particles in underfill for bimaterial with a straight edge.

The calculation for obtaining λ was done for all three material sets. Fig. 6 shows for the bimaterial with a straight edge. These bimaterial systems are composed of the silicon (chip) and underfill with effective properties of a composite. For all three material sets, the f parameter decreases as the in the underfill increases, and it decays to zero when two materials become identical, as expected. The material set 3 has the highest value since the material mismatches of the material set 3 are the most significant. The parameter λ does not change much until the f reaches 0.9 and it decreases suddenly near the f of 0. This trend was shown in the calculation of effective material properties for the material set 3. The parameters of stress singularity for the material set 1 is higher than one for the material set 2 before the f of 0.6 and it is low than the one for the material set 2 after the f of 0.6.

At the same time, we calculated the parameters of stress singularity for the bimaterial wedge with angular corners ($\theta_1 = \pi/2$ and $\theta_2 = 3\pi/2$) to compare the results of the straight edge of a bimaterial strip. The characteristic equation for the parameters is given Eqns. (14) and (15). We calculated the parameter for the material set 1, because we used material properties for the further interfacial stress analysis. Again, the λ parameter decreases as the f in the

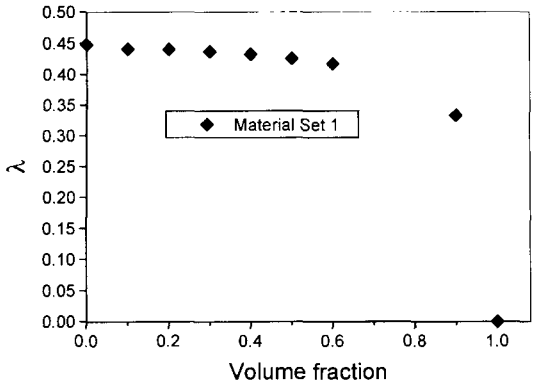

Fig. 7. Stress singularity vs. volume fraction of particles in underfill for angular corner of bimaterial wedge with the material set 1.

underfill increases, and it becomes zero when the f reaches 1.0. The value of λ for the bimaterial with an angular corner is higher than the one for a bimaterial with a straight edge. The results is shown in Fig. 7.

4.3 Interfacial Stresses of bimaterial Strips

We solved the problem of a bimaterial strip made of aluminum and molybdenum to verify our finite element model and to understand the effect of material properties. We compared the stresses, which we computed, with those obtained by Lau[30], and the interfacial stresses with the ones calculated by Suhir[31-33] and Kuo[34]. All the results match very closely. As expected, the elastic stresses are very high at the interface at or near the edge due to a singularity. Shear stress at the interface should be zero at the edge because of the traction-free boundary condition. In our calculations it is non-zero but small because of the approximation that occurs from the use of finite elements.

We studied the interfacial stresses in two kinds of finite bimaterial strips with two homogeneous constituents using three kinds of material sets given in Table 1 by increasing the in underfill. The dimensions of the models are given in Table 2.

At first, we calculated the interfacial stresses of the bimaterial strip 1, which has the thickness of chip is 4 times thicker than the one of underfill. The results are shown in Figs. 8-10. For material sets 1 and 2,

Table 2. Dimensions of bimaterial strips

		Length	Thickness
Strip 1	Chip	50 units	4 unit
	Underfill	50 units	1 unit
Strip 2	Chip	185 units	10 unit
	Underfill	185 units	1 unit

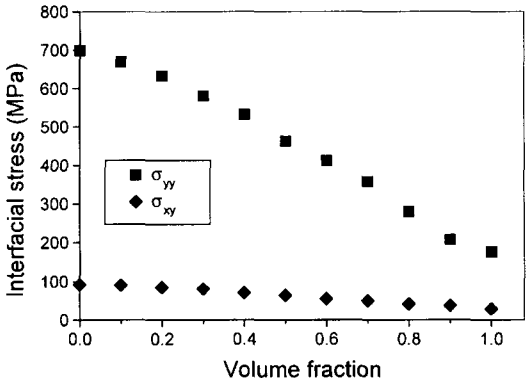

Fig. 8. Maximum interfacial stresses vs. volume fraction of particles in underfill for the bimaterial strip 1 with the material set 1.

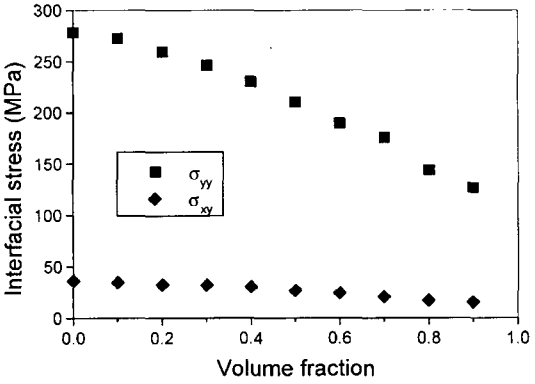

Fig. 9. Maximum interfacial stresses vs. volume fraction of particles in underfill for the bimaterial strip 1 with the material set 2.

as the f increases, the interfacial stresses decrease. When the f increases, the material mismatch is getting smaller and that leads the lower interfacial stresses. Since the material set 1 has the higher Young's modulus and Poisson's ratio, the interfacial stresses of the material set 1 are higher than the ones of the material set 2. The material set 3 has much higher interfacial stresses than the material set 1 and

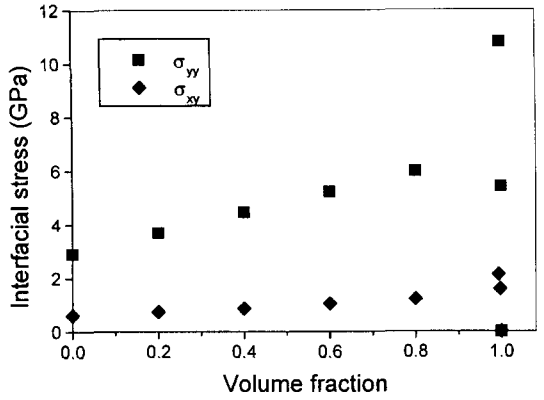

Fig. 10. Maximum interfacial stresses vs. volume fraction of particles in underfill for the bimaterial strip 1 with the material set 3.

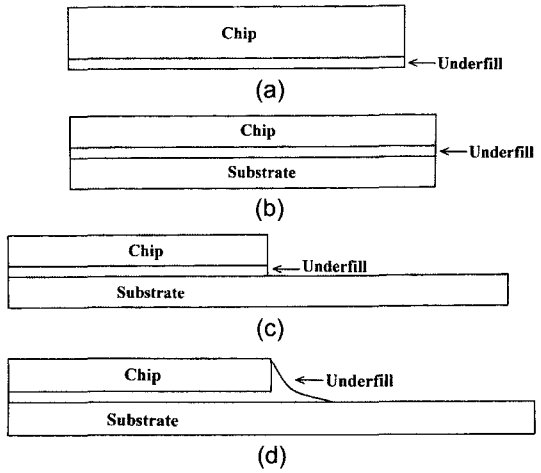

Fig. 11. Sketches of four different flip-chip models: (a) Bimaterial strip 2, (b) Three-layer case 1, (c) Three-layer case 2, and (d) Three-layer case 3.

2 and it shows the different trend than the other material sets. The interfacial stresses of the material set 3 increase as the f increases until 0.9 and after the point, they decrease rapidly. We can observe that the interfacial stress behavior depends on the material properties and when we have too large material mismatches, it is difficult to get precise results. Therefore, it can be stated that the material properties have large influences on the interfacial stress.

4.4 Interfacial Stresses of Three-layer Models

We considered the bimaterial strip 2, which has very long chip and underfill and the underfill is 10 times thinner than the chip, and three different three-layer models, which are more similar to the actual flip-chip device. The dimensions of the three-layer models are listed in Table 3. They include a three-layer model with the same length of strips (case 1), a three-layer model with long substrate and straight line of underfill edge (case 2), and a three-layer model with concave shaped curve for the long edge of underfill starting from at the top of the chip (case 3). The geometries of three-layer models are shown in Fig. 11. We considered the interfacial stresses by changing the f.

Fig. 12 gives the maximum interfacial stresses as a function of f in the underfill for four structures (the bimaterial strip 2 and the three-layer cases 1, 2 and 3) with the material set 1. The interfacial normal stress (σ_{yy}) for the bimaterial strip 2 and the three-layer cases 1 and 2 decreases as the f increases as shown in Fig. 12(a). Note that stresses in the three-

Table 3. Dimensions of the three-layer models

		Length	Thickness	Remarks
Case 1	Chip	185 units (14 mm)	10 units (0.762 mm)	equal length
	Underfill	185 units (14 mm)	1 unit (0.0762 mm)	
	Substrate	185 units (14 mm)	10 units (0.762 mm)	
Case 2	Chip	185 units (14 mm)	10 units (0.762 mm)	long substrate and a straight underfill edge
	Underfill	185 units (14 mm)	1 unit (0.0762 mm)	
	Substrate	370 units (28 mm)	10 units (0.762 mm)	
Case 3	Chip	185 units (14 mm)	10 units (0.762 mm)	underfill fillet starting at the top of chip
	Underfill	185 units (14 mm)	1 unit (0.0762 mm)	
	Substrate	370 units (28 mm)	10 units (0.762 mm)	

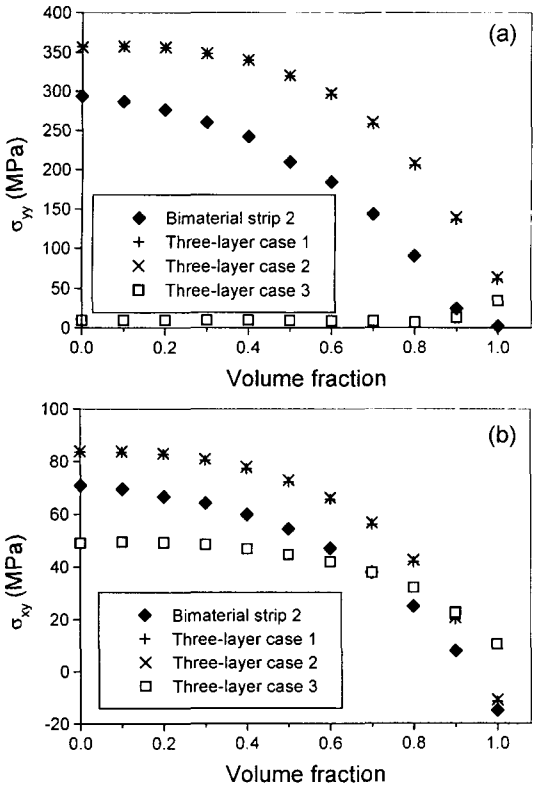

Fig. 12. Maximum interfacial stresses vs. volume fraction of particles in underfill for the bimaterial strip 2 and three-layer cases 1, 2 and 3 with the material set 1: (a) interfacial normal stress and (b) interfacial shear stress.

layer cases 1 and 2 are almost identical and have highest values. The bimaterial strip has lower interfacial normal stress, which the three-layer case 3 has the smallest interfacial normal stress. The normal stress for case 3 is nearly uniform.

Fig. 12(b) shows that the interfacial shear stress (σ_{yy}) decreases for all four cases as the f increases. Again, the shear stresses have highest values for the three-layer cases 1 and 2, followed by the stresses in the bimaterial strip 2. The smallest stresses are found in the case 3 for the being less or equal to 0.7. For larger than 0.7 the f curves cross. Note that at the f approaching unity the interfacial shear stress changes sign for bimaterial strip 2 and three-layer cases 1 and 2.

Silica has material properties similar to silicon (chip). Thus, putting more silica particles into the underfill reduces the mismatch of CTEs between the chip and underfill. That explains why the interfacial stresses decreases as the increases. The bimaterial strip and the three-layer cases 1 and 2 show the same trend but the three-layer cases have stresses higher by 20-30%, when compared with the bimaterial strip. These results show that an additional layer magnifies the interfacial stresses, while the length of third layer does not have a large contribution. The interfacial stresses are much smaller in the case 3 (where the chip edge is fully embedded in the underfill).

In summary, the near edge interfacial stresses have similar trends in the bimaterial strip and the three-layer cases 1, 2 and 3. Thus, it is reasonable to use a simple bimaterial strip model for a preliminary evaluation of the interfacial stresses in flip-chip devices.

5. Conclusions

1. The effective properties of underfill for several volume fractions of silica particles were calculated by Mori-Tanaka method for three different material sets, and the parameters of singularity for the bimaterial edge and the bimaterial wedge were calculated. It was found that the parameters of singularity decreased as the volume fraction of silica particles in underfill (f) increased. The singularity parameter for bimaterial wedge was higher than the one for the bimaterial edge.

2. Five different geometric models of flip-chip assembly involving two kinds of bimaterial strips and three kinds of three-layer models were considered under the assumption that the underfill is homogeneous. It was investigated numerically, using the finite element analysis, how stresses at underfill/chip interface were influenced by varying the volume fraction of silica particles in underfill and by the different geometric models of flip-chip devices. It was found that the higher volume fraction of particles in underfill leaded to lower interfacial stresses.

References

1. Z. Hashin and S. Shtrikman, "A variational approach

to the theory of the elastic behavior of multiphase materials", J. Mech. Phys. Solids, 11, 127 (1963).
2. B. Budiansky, "On the elastic moduli of some heterogeneous materials", J. Mech. Phys. Solids, 13, 223(1965).
3. R. Hill, "A self-consistent mechanics of composite materials", J. Mech. Phys. Solids, 13, 21 (1965).
4. T. Mori and K. Tanaka, "Average stress in matrix and average elastic energy of materials with misfitting inclusions", Acta Metall., 21, 571 (1973).
5. Y. Benveniste, "A new approach to the application of Mor-Tanaka's theory in composite materials", Mech. Mater., 6, 147 (1987).
6. R.M. Christensen, Mechanics of Composite Materials, Publ. Co., Malabar, Florida (1991).
7. T. Mura, Micromechanics of Defects in Solids, 2nd Ed., Martinus Nijhoff, Dordrecht (1987).
8. Z. Hashin, "Analysis of composite materials - A survey", J. Appl. Mech., 50, 481 (1983).
9. J. Qu and C.P. Wong, "Effective elastic modulus of underfill materials for flip-chip applications", IEEE Electronic Components and Technology Conf., 848(1998).
10. M.L. Williams, "The stress around a fault or crack in dissimilar media", Bull. Seismol. Soc. Am., 49, 199 (1959).
11. D.B. Bogy, "Edge-bonded dissimilar orthogonal elastic wedges under normal and shear loadings", ASME J. Appl. Mech., 35, 460 (1968).
12. D.B. Bogy and E. Sternberg, "The effect of couple-stresses on the corner singularity due to an asymmetric shear loadings", Int. J. Solids and Structures, 4, 159 (1968).
13. D.B. Bogy, "On the problem of edge-bonded elastic quarter planes loaded at the boundary", Int. J. Solids and Structures, 6, 1287 (1970).
14. J. Dundurs, "Discussion of 'edge-bonded dissimilar orthogonal elastic wedges under normal and shear loading", J. Appl. Mech., 36, 650 (1969).
15. C. Chung and J.W. Eischen, "The free-edges stress singularity at an interface between bilinear materials", Int. J. Solids and Structures, 28(1), 105 (1991).
16. M. Lee and I. Jasiuk, "Asymptotic expansions for the thermal stresses in bonded semi-infinite bimaterial strips", J. Electronic Packaging, 113, 173 (1991).
17. P.S. Theocaris, "The order of singularity at a multi-wedge corner of a composite plate", Int. J. Eng. Sci., 12, 107 (1974).
18. J.P. Dempsey and G.B. Sinclair, "On the singular behavior at the vertex of a bi-material wedge", J. Elasticity, 11(3), 317 (1981).
19. H.L. Groth, "Stress singularities and fracture at interface corners in bonded joints", Int. J. Adhesion and Adhesives, 8(2), 107 (1988).
20. L. Gu and Belytschko, "A numerical study of stress singularities in a two-material wedge", Int. J. Solids and Structures, 31(6), 865 (1994).
21. S.S. Pageau, P.F. Joseph and S.B. Biggers, "Finite element analysis of anisotropic materials with singular inplane stress fields", Int. J. Solids and Structures, 32(5), 571 (1995).
22. J.C.W. Vroonhoven, "Effects of adhesion and delamination on stress singularities in plastic-packaged integrated circuits", Trans. ASME, 115, 28 (1993).
23. X.J. Fan, H.B. Wang and T.B. Lim, "Investigation of the underfill delamination and cracking inflip-chip modules under temperature cyclic loading", ECTC, 994 (1999).
24. W. Wang and I. Jasiuk, "Effective elastic constants of particulate composites with inhomogeneous interphases", J. Composite Materials, 32(15), 1391 (1998).
25. S. Michaelides and S.K. Sitaraman, "Die cracking and reliable die design for flip-chip assemblies", IEEE Trans. Adv. Packaging, 22(4), 602 (1999).
26. C.E. Hanna and S.K. Sitaraman, "Role of underfill materials and thermal cycling on die stresses", Proc. Adv. Electronic Packaging InterPACK 99, 26-1, 795 (1999).
27. C.P. Yeh, W.X. Zhou and K. Wyatt, "Parametric finite-element analysis of flip-chip structures", Int. J. Microcircuit Electronic Packagings, 19(2), 120 (1996).
28. R.K. Mahidhara, V. Solberg, T. Distefano and S. Greathouse, "Solder joint integrity in Tessera's μBGA package", Design and Reliability of Solder and Solder Inerconnections, 405 (1997).
29. D.B. Bogy and K.C. Wang, "Stress singularities at interface corners in bonded dissimilar isotropic elastic materials", Int. J. Solids and Structures, 7, 993 (1971).
30. J.H. Lau, "A note on the calculations of thermal stresses in electronic packaging by finite elements methods", ASME J. Electronic Packaging, 111, 313 (1989).
31. E. Suhir, "Stresses in bi-metal thermostat", ASME J. Appl. Mech., 53, 657 (1986).
32. E. Suhir, "Interfacial stresses in bimetal thermostats", ASME J. Appl. Mech., 56, 595 (1989).
33. E. Suhir, "Thermally induced interfacial stresses in elongated bimetal plates", Appl. Mech. Rev., 42(11), S253 (1989).
34. A.Y. Kuo, "Thermal stresses at the edge of bimetallic thermostat", ASME J. Appl. Mech., 56, 585 (1989).